RSC Advances

ROYAL SOCIETY OF CHEMISTRY

www.rsc.org/advances

Controlled Fabrication of Bi-functional Fe_3O_4@SiO_2@Gd_2O_3:Yb,Er Nanoparticles and Their Magnetic, Up-conversion Luminescent Properties

Peng Jing,[1] *Qin Wang,*[1] *Baocang Liu,*[1,2] *Guangran Xu,*[1] *Yanbing Zhang,*[1] *Jun Zhang*[1,2,3]* *and Gejihu De*[4]

[1]College of Chemistry and Chemical Engineering, Inner Mongolia University, Hohhot 010021, P.R. China

[2]College of Life Sciences, Inner Mongolia University, Hohhot 010021, P.R. China

[3]Inner Mongolia Key Lab of Nanoscience and Nanotechnology, Hohhot 010021, P.R. China

[4]College of Chemistry and Environment Science, Inner Mongolia Normal University, Hohhot 010022, China

* Corresponding author: J. Zhang, Tel.: 0086 471 4992175; Fax: 0086 471 4992278; Email: cejzhang@imu.edu.cn

Abstract

We develop a facile layer-by-layer deposition process to create bi-functional Fe_3O_4@SiO_2@Gd_2O_3:Yb,Er nanostructures composed of magnetic Fe_3O_4 cores, variable SiO_2 mid-layers, and magnetic and up-converting Gd_2O_3 shells. The synthetic process is well-controlled and the obtained Fe_3O_4@SiO_2@Gd_2O_3:Yb,Er nanoparticles show relative monodispersity and exhibit tunable magnetic and up-conversion luminescence depending on the thickness of SiO_2 mid-layers. The influences of SiO_2 mid-buffer-layers on morphology, magnetism, and up-conversion luminescence are well addressed. The obtained bi-functional Fe_3O_4@SiO_2@Gd_2O_3:Yb,Er nanoparticles may be potentially applicable in magnetic, fluorescent, and biological applications. The synthetic route may be employed for fabricating other multifunctional nanostructures.

Keywords: Fe_3O_4, Gd_2O_3:Yb, Er, Bi-functional nanoparticles, Magnetism, Up-conversion luminescence.

1. Introduction

Magnetic and luminescent bi-functional nanomaterials have attracted great attention in recent years owing to their potential application in biological fields such as in fluorescent targeting, multimodal imaging, and drug delivery [1-3]. In the choice of luminescent nanomaterials for labeling, targeting and imaging, up-conversion nanoparticles (UCNPs) possess lots of advantages such as high fluorescence quantum yields, low toxicity, long lifetimes, and high stability in comparison with quantum dots and organic dyes [2]. UCNPs can convert near-infrared wavelength radiation to shorter wavelength radiation through a two-photon or multi-photon mechanism [4-8]. Because UCNPs can be luminous under the excitation of NIR radiation, the strong background autofluorescence from biological entities, which may decrease the sensitivity of detection, can be largely avoided [9, 10]. Thus, the biological detection and imaging based on UCNPs with NIR radiation may have deeper penetration depth in tissues, enabling better detection and imaging sensitivity and resolution [11]. To realize the magnetic feasibility simultaneously in UCNPS, magnetic Fe_3O_4 nanoparticles with large magnetic moment are expected to be integrated into such UCNPs to achieve bi-functional entities through various synthetic strategies of core-shell architecture, surface decoration, and composite integration for multimodal applications.

To date, there have been some reports for constructing bi-functional nanostructures that were made up of Fe_3O_4 and UCNPs. The Fe_3O_4 and UCNPs could be combined with each other by a cross-linker anchoring process or via a facile aqueous-based co-precipitation approach under mild conditions [3, 12-15]. In these demonstrations, if the UCNPs are chosen as cores [16], their luminescent intensity may be suppressed to some extent due to the coating of

outer layers. Meanwhile, if the UCNPs are direct in contact with Fe_3O_4, their luminescence may be decreased as the direct contact can cause fluorescence quenching [17]. Therefore, a SiO_2 mid-layer between Fe_3O_4 and UCNPs is needed and the core-shell structure is widely endowed in such bi-functional nanostructures. These multifunctional nanostructures can be used not only in MRI and UCL imaging, but also in CT imaging due to their large atomic number and high X-ray absorption coefficient of lutetium. Besides, amino-modified surface and mesoporous silica outer shell can also endow them positive aspects for loading and controlled release of ibuprofen (IBU). It is revealed that in such core-shell nanostructures, SiO_2 layer has a significant influence on their structure, morphology and property. Herein, we fabricate bi-functional core-shell Fe_3O_4@SiO_2@Gd_2O_3:Yb,Er nanostructures composed of Fe_3O_4 cores, SiO_2 mid-layers and Gd_2O_3 shells through a facial layer-by-layer deposition approach. The obtained bi-functional core-shell Fe_3O_4@SiO_2@Gd_2O_3:Yb,Er nanostructures exhibit uniform spherical morphology and excellent magnetic and fluorescent properties. The thickness of SiO_2 mid-layers is found to have great effects on the magnetic and luminescent properties of Fe_3O_4@SiO_2@Gd_2O_3:Yb,Er nanoparticles. An appropriate thickness of SiO_2 mid-buffer-layers may result in higher luminescent intensity of bi-functional core-shell Fe_3O_4@SiO_2@Gd_2O_3:Yb,Er nanoparticles and make them retain good magnetic responsive property simultaneously. The obtained bi-functional Fe_3O_4@SiO_2@Gd_2O_3:Yb,Er nanoparticles may have potential values in magnetic, fluorescent, and biological applications. The synthetic route may also be applicable for fabricating other multifunctional nanostructures.

2. Experimental

2.1. Chemicals

Tetraethyl orthosilicate (TEOS) was purchased from Sinopharm Chemical Reagent Co., Ltd. $FeCl_3 \cdot 6H_2O$, sodium acetate, trisodium citrate, ammonia solution (25-28 wt%), urea, ethylene glycol, and absolute ethanol were obtained from Tianjin Windship Chemistry Technological Co., Ltd. $Gd(NO_3)_3 \cdot 6H_2O$, $Yb(NO_3)_3 \cdot 5H_2O$, $Er(NO_3)_3 \cdot 5H_2O$ and 3-Aminopropyl-triethoxysilane (APTES) were purchased from Aladdin. All chemicals were used as received without further treatment. Deionized water was used for all experiments.

2.2. Preparation of materials

2.2.1. Synthesis of uniform Fe_3O_4 nanoparticles

Fe_3O_4 nanoparticles were prepared according to the literature reported previously [18]. Briefly, $FeCl_3 \cdot 6H_2O$ (1.3 g), sodium acetate (2 g), and trisodium citrate (0.5 g) were dissolved in 40 mL ethylene glycol with continuous stirring for 1 h. Then, the solution was transferred into a Teflon-lined stainless-steel autoclave, the autoclave was heated to 200°C and maintained for 10 h. After it was cooled to room temperature, the obtained product was washed with ethanol and deionized water several times.

2.2.2. Synthesis of Fe_3O_4@SiO_2 nanoparticles

The Fe_3O_4@SiO_2 nanoparticles were prepared by a versatile Stöber sol-gel method [18]. In a typical synthesis, 0.1 g as-prepared Fe_3O_4 nanoparticles were dispersed in a mixture of ethanol (187 mL), deionized water (47 mL), and ammonia solution (3.5 mL) under ultrasonication for 30 min. Then, different amount of TEOS precursor was added to the solution dropwise, the reaction was proceeded under mechanical stirring for 10 h at room temperature. After that, the product was collected by a magnet and washed by ethanol and

deionized water several times. To obtain the samples with different thicknesses of SiO_2 mid-layers, 0.53, 2.67, 5.34, 13.35, and 18.69 mL of TEOS were used.

2.2.3. Synthesis of Fe_3O_4@SiO_2@Gd_2O_3:Yb,Er nanoparticles

To incorporate Gd_2O_3:Yb, Er onto SiO_2 layers [19], the synthetic process was carried out and described below: 0.701 g of $Gd(NO_3)_3 \cdot 6H_2O$, 0.079 g $Yb(NO_3)_3 \cdot 5H_2O$, and 0.006 g $Er(NO_3)_3 \cdot 5H_2O$ and 2.241 g urea were mixed and dissolved in 38 mL deionized water. 0.15 g Fe_3O_4@SiO_2 was then added and the solution was hold for 4 h at 85°C. The final product was separated by a magnet and washed with deionized water several times. The product was then dried at 80 °C for 12 h and calcined at 800°C for 2 h under the protection of argon. The samples with different thickness of SiO_2 mid-layers prepared using the TEOS precursor of 0.53, 2.67, 5.34, 13.35, and 18.69 mL were denoted as S1, S2, S3, S4, and S5.

2.2.4. Surface modification of Fe_3O_4@SiO_2@Gd_2O_3:Yb,Er nanoparticles

0.1g Fe_3O_4@SiO_2@Gd_2O_3:Yb,Er, 0.1 ml APTES were mixed in 50 ml ethanol, the solution was refluxed at 80 °C for 12h. The product was separated by a magnet and washed with ethanol several times.

2.3. Characterization

XRD was used to characterize the phase structure of the samples. Measurements were performed using a PANalitical EMPYREAN X-ray diffractometer operated at 40 kV and 40 mA using Cu Ka radiation (k = 0.15406 nm). Scanning electron micrographs were recorded with a JEOL-JSM 6700-F field-emission scanning electron microscope (FE-SEM). Samples for SEM measurements were deposited on silicon substrates and coated with a 5 nm Pt for characterization TEM characterization was performed on a Hitachi H-800 system operated at

an acceleration voltage of 200 kV. Samples for TEM analysis were prepared by drying a drop of microspheres dispersion on an amorphous carbon coated copper grid for observation. The up-conversion luminescence spectra were recorded on an Edinburgh FLS-920 instrument with a 980 nm diode laser as the excitation source. The magnetization curves of different samples were measured with a vibrating sample magnetometer (Nanjing university Co., Ltd, HH-15).

3. Result and discussion

The synthetic procedures for Fe_3O_4@SiO_2@Gd_2O_3:Yb,Er nanostructures are presented in scheme 1. As illustrated in Scheme 1, magnetic Fe_3O_4 nanoparticles were firstly prepared and used as starting cores. Then, a layer of SiO_2 was coated on Fe_3O_4 cores to achieve Fe_3O_4@SiO_2 nanostructures. Depending on the amount of TEOS precursor used for SiO_2 coating, the obtained Fe_3O_4@SiO_2 nanostructures have variable shell thickness and morphologies. Then, by coating a layer of up-converting Gd_2O_3:Yb,Er, the bi-functional Fe_3O_4@SiO_2@Gd_2O_3:Yb,Er nanostructures were obtained. The synthetic process was monitored by XRD characterization. Figure 1 shows the XRD patterns of Fe_3O_4, Fe_3O_4@SiO_2 (the amount of TEOS precursor fixed at 5.34 mL) and Fe_3O_4@SiO_2@Gd_2O_3:Yb,Er (S3). The characteristic diffraction peaks in Figure 1 can be well indexed to face centered cubic Fe_3O_4 (JCPDS No: 19-0629), cubic Gd_2O_3 (JCPDS No: 88-2165), and SiO_2 (JCPDS No: 29-0085). Obviously, the diffraction peaks corresponding to Fe_3O_4 become weaker after depositing the SiO_2 layer. When Gd_2O_3:Yb,Er layer was subsequently coated on Fe_3O_4@SiO_2, the diffraction peaks indexed to Fe_3O_4 can be hardly seen and the diffraction peaks ascribed to SiO_2 become weaker as well. This evidently proves the successful construction of core-shell Fe_3O_4@SiO_2@Gd_2O_3:Yb,Er nanostructures. From the XRD data in Figure 2, the full width at

half maximum of Gd_2O_3 gradually narrows as the amount of added TEOS increases to 5.34 ml, then broadens as added amount further increases indicating the good crystallinity of Gd_2O_3 in S2, S3, and S4. The crystallinity of Gd_2O_3 in S3 is better than that in S2 and S4, while they are similar in S2 and S4. However, for S1 and S5, the characteristic diffraction peaks of Gd_2O_3 are relatively weak. Besides, there are also some diffraction peaks (they are noted as ＊) appeared in S1, which can be indexed to gadolinium iron oxide (JCPDS No: 78-0451 and No: 72-0141). The distinctions in crystallinity of Gd_2O_3 in S1 and S5 (Figure 2a and e) will be discussed below combined with the corresponding TEM characterization.

The size and morphology of Fe_3O_4, $Fe_3O_4@SiO_2$, and $Fe_3O_4@SiO_2@Gd_2O_3$:Yb,Er nanostructures are shown in Figures 3 and 4. From the SEM images in Figures 3a-f, it can be seen that Fe_3O_4 nanoparticles are quite uniform and possess spherical morphology. The $Fe_3O_4@SiO_2$ nanoparticles show relative monodispersity with little aggregation. After coating Gd_2O_3:Yb,Er on $Fe_3O_4@SiO_2$ nanoparticles, the morphology of the obtained $Fe_3O_4@SiO_2@Gd_2O_3$:Yb,Er (Figure 4) is similar as the corresponding $Fe_3O_4@SiO_2$ nanoparticles, but the size is largely influenced by the quality of subsequent coating [20].

TEM characterization is conducted to further investigate the interior structure of the nanoparticles (Figure 5). The mid-layer of SiO_2 and the outer layer of Gd_2O_3:Yb,Er can be clearly observed, combined with the XRD data, indicating that the successful synthesis of core-shell $Fe_3O_4@SiO_2@Gd_2O_3$:Yb,Er nanoparticles. The sizes of the nanoparticles increase when more TEOS precursor is used in the coating process. High angle annular dark eld-scanning transmission electron microscopy (HAADF-STEM) and elemental mapping have also been performed to reveal the elemental distribution in the microspheres. The

HAADF-STEM images indicate that the Fe_3O_4@SiO_2@Gd_2O_3:Yb,Er (S3) possesses well defined core-shell structure (Figure 6 a-c). The EDX elemental mapping of Fe, O, Si, Gd, Er, and Yb (Figure 6 d-i) further confirm the structure as these elements are well dispersed at specific location in the core-shell structure. The line scanning and mapping results (Fig. 7A) indicate that the elements Fe, O, Si, Gd, Er and Yb are spread evenly throughout the whole spheres. Meanwhile, the Si, Gd, Er and Yb are almost completely located on the outermost surface of the microspheres. The energy-dispersive spectrum (EDS) result (Fig. 7B) also reveals that Fe, O, Si, Gd, Er and Yb are contained in the sample. The size and morphology of Fe_3O_4@SiO_2@Gd_2O_3:Yb,Er nanoparticles with different thickness of SiO_2 mid-layer can be tuned. From the XRD data (Figure 2), the crystallinity of Gd_2O_3 in S1 and S5 are relatively low. A very thin layer of SiO_2 which cannot act as an effective spacer means that some Fe_3O_4 are still exposed (S1). As a result, a large portion of Gd_2O_3 react with Fe_3O_4 at 800°C during the synthesis of Gd_2O_3:Yb, Er [21]. The severe aggregation and the breakdown of spherical morphology in TEM image (Figure 5b) may also indicate the occurrence of this reaction. However, with a thick SiO_2 layer (S5), the size of Fe_3O_4@SiO_2@Gd_2O_3:Yb,Er nanoparticles is about 200 nm, which is twice as large as S1. More aggregated particles will form at the same time. Like cerium oxide, there may also occur a chemical reaction between gadolinium oxide particles or gadolinium precursor and SiO_2 [22]. Larger surface area of SiO_2 makes more gadolinium take part in the reaction under the same molar ratio of (Gd_2O_3)/(Fe_3O_4@SiO_2), finally leading to the low crystallinity of Gd_2O_3 (S5). This phenomenon can be proven by HADDF-STEM (Fig 8A) and EDX elemental mapping images (Fig 8B) of Fe_3O_4@Gd_2O_3:Yb,Er after removing SiO_2 from Fe_3O_4@SiO_2@Gd_2O_3:Yb,Er nanoparticles

(S5). There still exists some Si element close to gadolinium element even after removing SiO_2 by 2M NaOH twice. This left part of Si could be the section that reacts with gadolinium. Because the reacted Si does not exist in the type of SiO_2, they cannot be removed by NaOH. This is a powerful proof for the chemical reaction between gadolinium oxide particles or gadolinium precursor and SiO_2. That is to say too thin or too thick SiO_2 layer is not helpful for crystallization of Gd_2O_3.

The up-conversion luminescence (UCL) spectra of Fe_3O_4@SiO_2@Gd_2O_3:Yb,Er with different thicknesses of SiO_2 layer under 980 nm NIR excitation are shown in Figure 9A. There are three emission band appeared in the spectra. Figure 9B displays the energy level diagrams of Er^{3+} and Yb^{3+} ions and possible mechanism accounting for the four emissions under 980 nm excitation. The green emission band in 525 nm and 560 nm are attributed to the transitions $^2H_{11/2}$ to $^4I_{15/2}$ and $^4S_{3/2}$ to $^4I_{15/2}$ and the red emission band in 662 nm corresponds to the $^4F_{9/2}$ to $^4I_{15/2}$ transition[15]. As the molar ratio of Yb/Er in Gd_2O_3:Yb,Er is 10:1, the dominant emission is in red region, which can be seen by naked eye as well [23]. The inset in Figure 9A shows the relationship between the thickness of SiO_2 mid-layer and luminescence intensity at 662 nm of Fe_3O_4@SiO_2@Gd_2O_3:Yb,Er (S1-S5). The intensity of luminescence is low at first (S1), then increases rapidly (S2) and reaches the highest point (S3), then decrease a little (S4), at last it decreases to nearly initial level (S5). There are two reasons accounting for this phenomenon: (1) direct contact between Fe_3O_4 and Gd_2O_3:Yb,Er will cause strong quenching effect on luminescence, this negative effect is weakened to some extent when Fe_3O_4 is coated by SiO_2, so the luminescent intensities from S1 to S3 increase with the increase of the thickness of SiO_2 layer; (2) Gd_2O_3 acts as matrix material for luminescence, so better

crystallinity is significant for well-defined optical properties[24, 25]. The crystallinity of Gd_2O_3 in S1, S2 and S3 follows this order: S3>S2>S1. However, for S3 to S5, the luminescent intensities from S3 to S5 decrease with the further increase of the thickness of SiO_2 layer, a thicker SiO_2 mid-layer do not mean a better optical performance as before. The quenching effect is negligible, the crystallinity of Gd_2O_3 is the main reason as the crystallinity of Gd_2O_3 in S3, S4 and S5 follows this order: S3>S4>S5. The large particle size and serve aggregation, suppresses the luminescence as well.

The magnetic property of Fe_3O_4@SiO_2@Gd_2O_3:Yb,Er nanoparticles is also examined as shown in Figure 10. The magnetization values are measured to be 42.90, 4.15, and 4.12 emu/g for Fe_3O_4, Fe_3O_4@SiO_2 (the amount of TEOS precursor is fixed at 5.34 mL), and Fe_3O_4@SiO_2@Gd_2O_3:Yb,Er (S3). The huge decrease in Ms value (42.90 to 4.15 emu/g) is caused by coating a thick nonmagnetic SiO_2 layers (curve b in Figure 10A) [15]. However, Ms value of Fe_3O_4@SiO_2 and Fe_3O_4@SiO_2@Gd_2O_3:Yb,Er (4.15 and 4.12 emu/g) are nearly the same. A thin Gd_2O_3:Yb,Er shell which can be clearly seen from the TEM image (Figure 5d) is formed on the outer layer, causing little influence on the Ms value. The Ms values of Fe_3O_4@SiO_2@Gd_2O_3:Yb,Er with different thickness of SiO_2 mid-layers are 12.89, 4.82, 4.12, 3.09, and 2.22 emu/g, respectively (Figure 10B). This is consistent with the thicknesses of SiO_2 mid-layers in S1-S5. Thick SiO_2 mid-layers may cause the decrease of Ms value. To exhibit a better performance in biological applications, higher luminescent intensity and excellent magnetic property are needed. The dual properties of Fe_3O_4@SiO_2@Gd_2O_3:Yb,Er are demonstrated by digital photographs in Figure 11. The Fe_3O_4@SiO_2@Gd_2O_3:Yb,Er nanoparticles can be easily collected by an external magnetic field near a vessel after several

minutes. The red up-converting emitting light of the aqueous solution with dispersed Fe_3O_4@SiO_2@Gd_2O_3:Yb,Er nanoparticles collected a magnetic field can be easily seen. Therefore, the bi-functional Fe_3O_4@SiO_2@Gd_2O_3:Yb,Er nanoparticles with good magnetic and luminescent properties may find a wide range of applications in magnetic, fluorescent, and biological applications.

To further expand its application, surface modification with amino group is an excellent tool as it can be linked to specific drug or proteins. Infrared spectroscopy of the sample S3 before and after surface modification is shown in Figure 12. Bands at 3406 $cm^{-1}$and 1621 cm^{-1} are attributed to bending vibration of absorbed molecular water. The Bands at 1093 cm^{-1}, 626 cm^{-1} and 428 cm^{-1} correspond to Si-O bond, Gd-O bond and Fe-O bond. The carboxyl salts belonged to citric acid which was located on the surface of Fe_3O_4 has a absorption band at 1395 cm^{-1}, After surface modification with amino groups (Fig 12b), the absorption of asymmetrical and symmetrical stretching of -CH_2- which was linked to -NH_2 are presented at 2912 cm^{-1} and 2837 cm^{-1}, suggesting that the nanoparticle is modified with amino groups successfully. As described above, these amino group modified nanoparticles may be applied for drug loading and further move to a specific area to under an external magnetic field [3]. Moreover, Another significant application is cell imaging such as the HeLa cells [26]. Specific protein is attached onto the nanoparticles and then through the recognition to the specific cells cell-imaging is achieved.

4. Conclusion

In summary, bi-functional core-shell Fe_3O_4@SiO_2@Gd_2O_3:Yb,Er nanoparticles composed of Fe_3O_4 cores, SiO_2 mid-layers and Gd_2O_3 shells were synthesized through a relatively

simple layer-by-layer deposition process. The obtained Fe_3O_4@SiO_2@Gd_2O_3:Yb,Er nanoparticles show relative monodispersity and possess magnetic and up-conversion luminescent properties with good water solubility. It is revealed that the SiO_2 mid-layer has a great effect on the size, morphology and magnetic and luminescent properties of final bi-functional Fe_3O_4@SiO_2@Gd_2O_3:Yb,Er nanoparticles. A suitable SiO_2 mid-layer may help to gain higher luminescence while maintaining its magnetic property simultaneously. The bi-functional core-shell Fe_3O_4@SiO_2@Gd_2O_3:Yb,Er nanoparticles may have potential application in MRI, biolabeling, and bioimaging.

Acknowledgement

This work was supported by NSFC (21261011), NSFC (21467019), NSFC (21201097), Program for New Century Excellent Talents in University (NCET-10-0907), Application Program from Inner Mongolia Science and Technology Department (2011401), Inner Mongolia Talent Development Fund, and Inner Mongolia "Grassland Talent" Program (12101619) and Natural Science Foundation of Inner Mongolia Autonomous Region of china (2014MS0506).

References

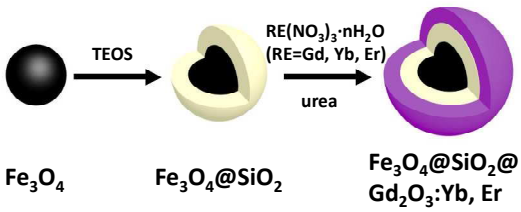

Scheme 1. Schematic illustration shows the procedures for synthesis of

Fe_3O_4@SiO_2@Gd_2O_3:Yb,Er nanoparticles.

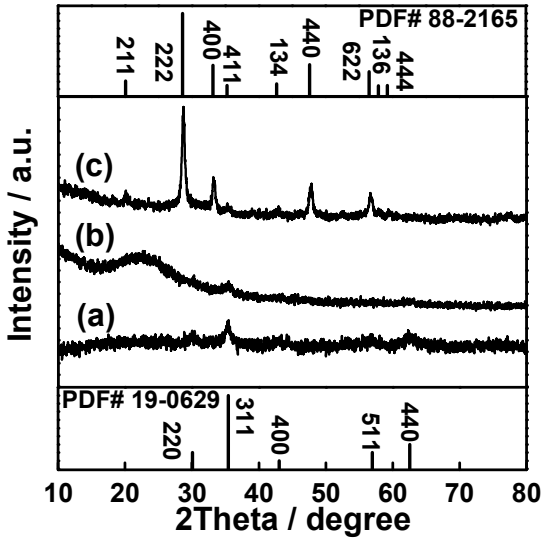

Figure 1. XRD patterns of (a) Fe_3O_4, (b) Fe_3O_4@SiO_2 (the amount of TEOS fixed at 5.34 mL) and (c) Fe_3O_4@SiO_2@Gd_2O_3:Yb,Er nanoparticles (S3).

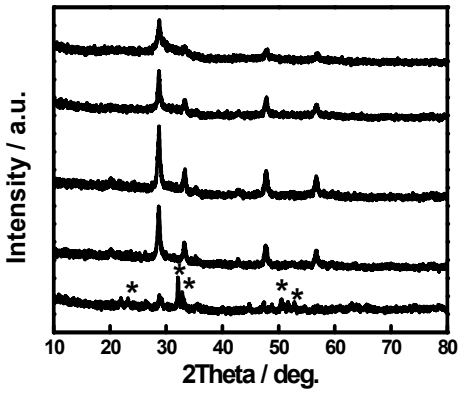

Figure 2. XRD patterns of Fe_3O_4@SiO_2@Gd_2O_3:Yb, Er with different thickness of SiO_2mid-layer: (a) S1, (b) S2, (c) S3, (d) S4, and (d) S5 obtained using 0.53, 2.67, 5.34, 13.35, and 18.69 mL TEOS as precursor.

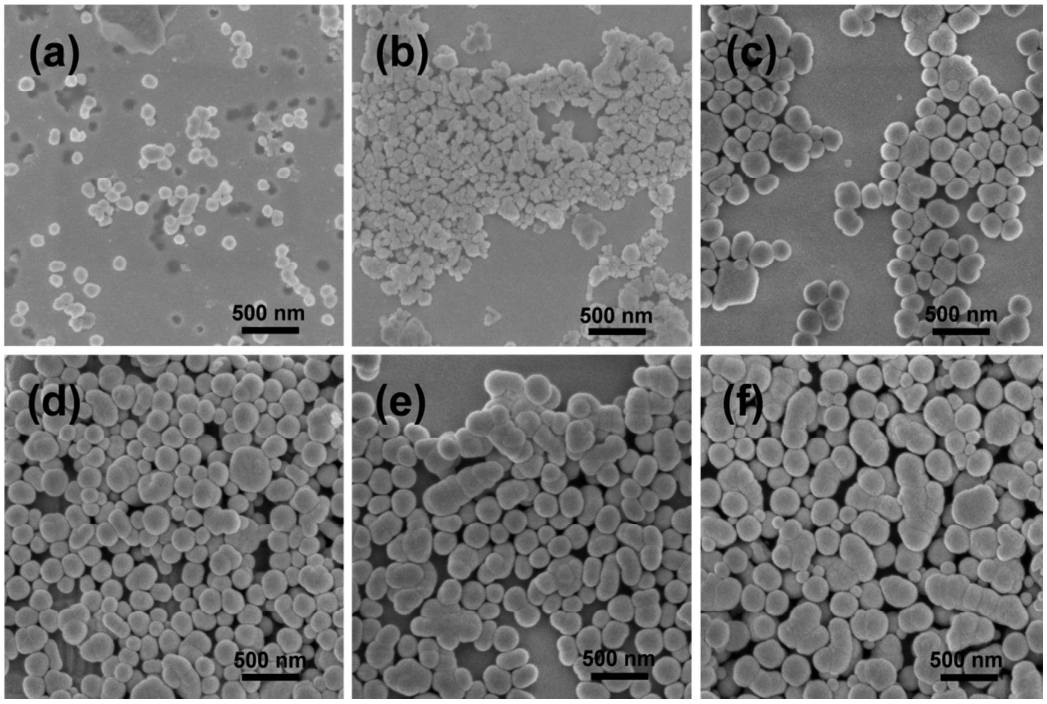

Figure 3. SEM images of Fe_3O_4 (a) and Fe_3O_4@SiO_2 nanoparticles with different thickness of SiO_2 shells obtained using (b) 0.53, (c) 2.67, (d) 5.34, (e) 13.35, and (f) 18.69 mL TEOS as precursor.

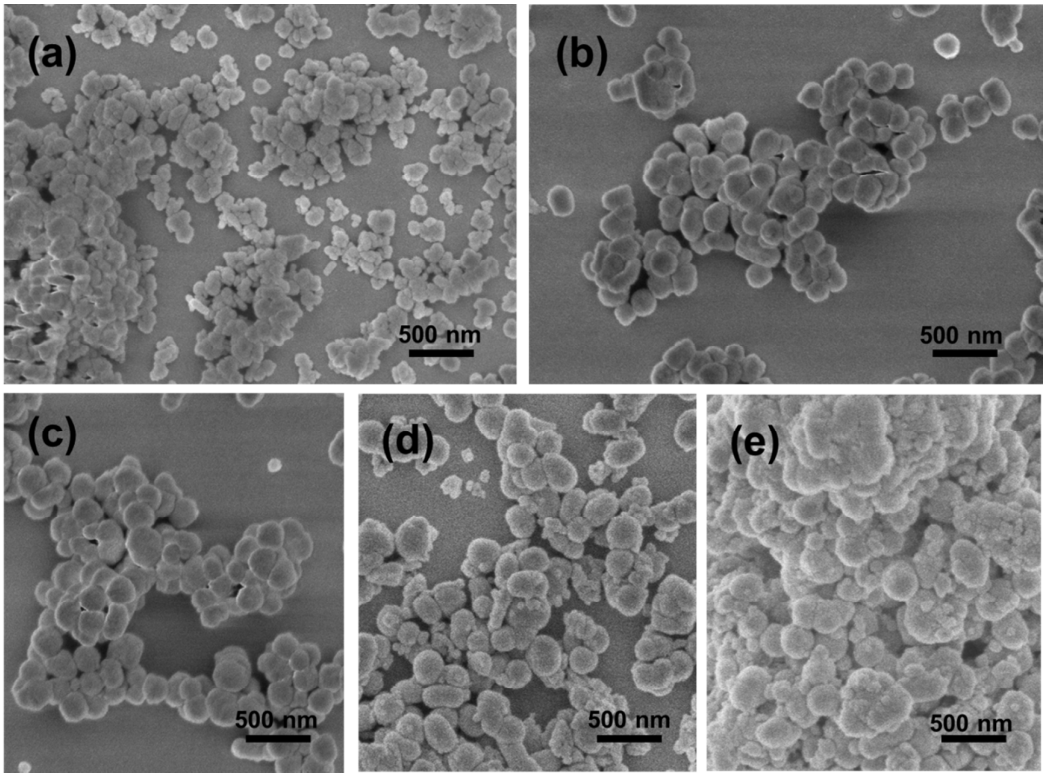

Figure 4. SEM images of Fe_3O_4@SiO_2@Gd_2O_3:Yb,Er with different thickness of SiO_2 mid-layers obtained using (a) 0.53, (b) 2.67, (c) 5.34, (d) 13.35, and (e) 18.69 mL TEOS as precursor.

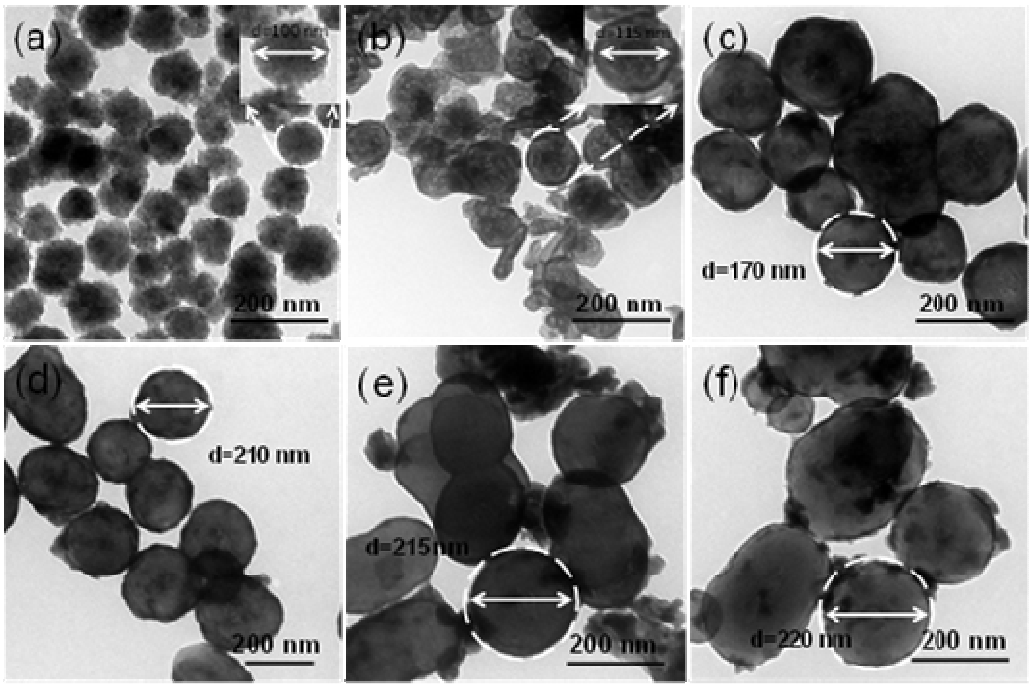

Figure 5. TEM images of Fe_3O_4 (a) and Fe_3O_4@SiO_2@Gd_2O_3:Yb,Er nanoparticles with different thickness of SiO_2 mid-layers obtained using (b) 0.53, (c) 2.67, (d) 5.34, (e) 13.35, and (f) 18.69 mL TEOS as precursor.

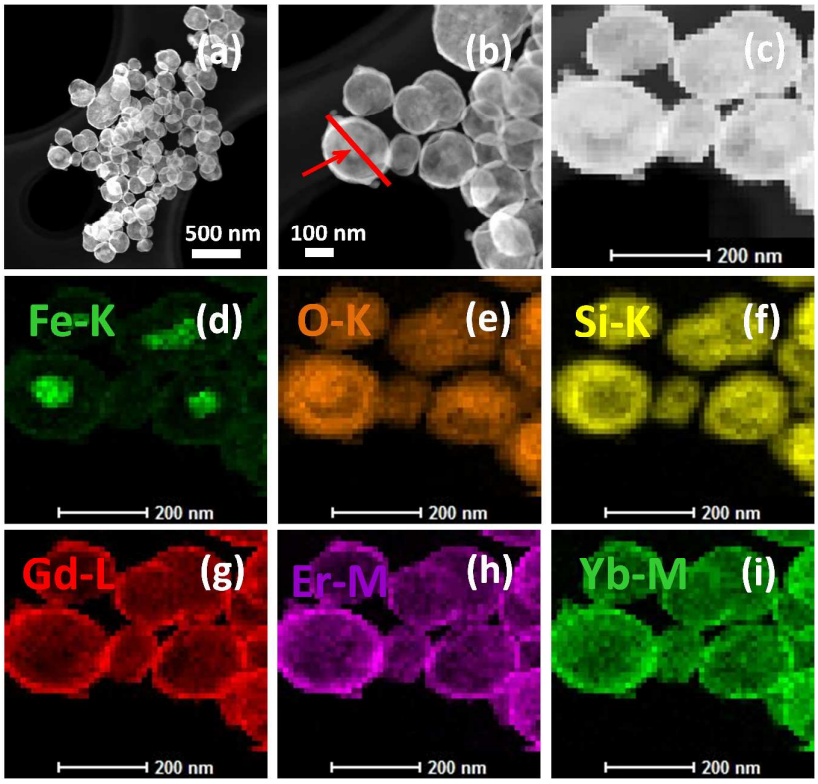

Figure 6. (a-c) HAADF-STEM images of Fe_3O_4@SiO_2@Gd_2O_3:Yb,Er (S3) and (d-i) EDX elemental mapping of Fe, O, Si, Gd, Er and Yb in Fe_3O_4@SiO_2@Gd_2O_3:Yb,Er (S3).

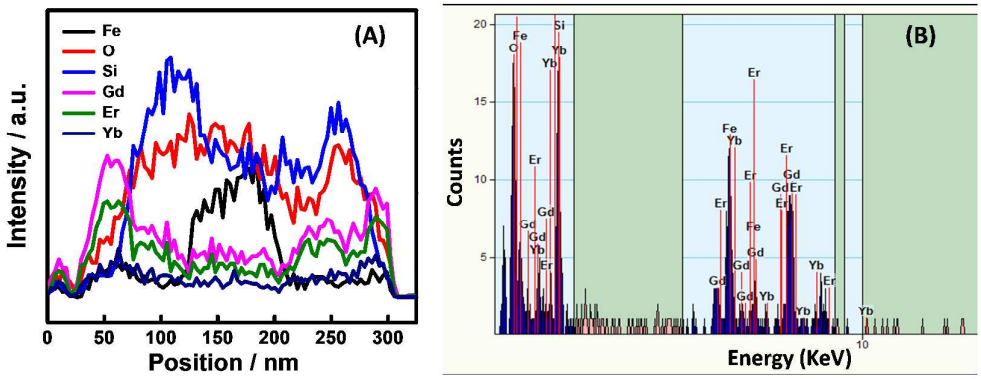

Figure 7. (A) line scanning profiles of Fe, O, Si, Gd, Er and Yb in Fe_3O_4@SiO_2@Gd_2O_3:Yb,Er (S3) recorded along the line shown in Fig 6c, (B) EDS spectrum of Fe_3O_4@SiO_2@Gd_2O_3:Yb,Er (S3) recorded for the given point that the arrow indicated in Fig 6c.

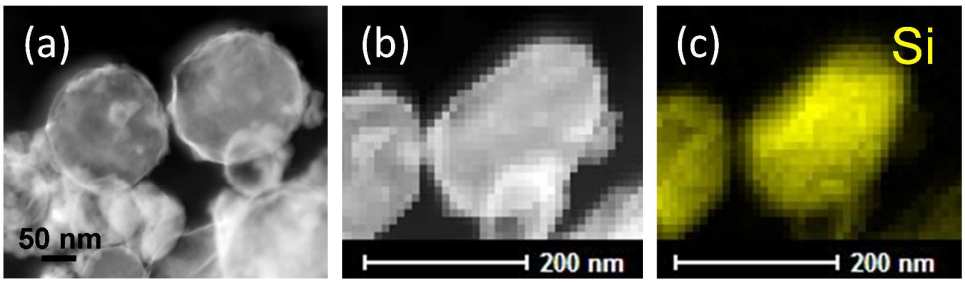

Figure 8 (a-b) HAADF-STEM images of Fe_3O_4@Gd_2O_3:Yb,Er (S5) and (c) EDX elemental mapping of Si in Fe_3O_4@Gd_2O_3:Yb,Er (S5).

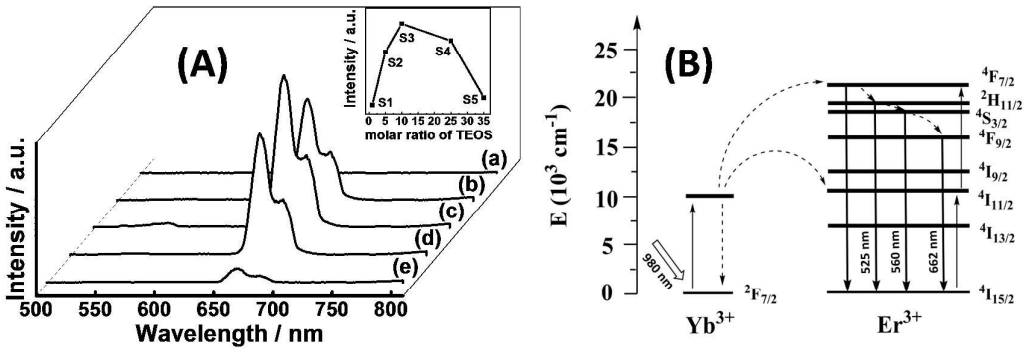

Figure 9. Up-conversion luminescent spectra of (A) Fe_3O_4@SiO_2@Gd_2O_3:Yb,Er with different thickness of SiO_2 mid-layers obtained using (a) 0.53, (b) 2.67, (c) 5.34, (d) 13.35, and (e) 18.69 mL TEOS as precursor for preparation. The inset shows the relationship of the thickness of SiO_2 mid-layer with luminescence intensity at 662 nm for Fe_3O_4@SiO_2@Gd_2O_3:Yb,Er nanoparticles. (B) The proposed energy transfer mechanism for up-conversion process of Fe_3O_4@SiO_2@Gd_2O_3:Yb,Er under 980 nm excitation.

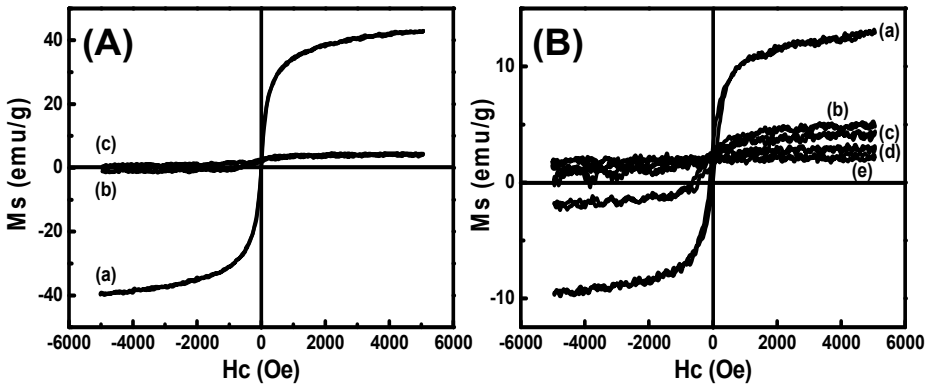

Figure 10. (A) Magnetization curves of (a) Fe_3O_4, (b) Fe_3O_4@SiO_2, and (c) Fe_3O_4@SiO_2@Gd_2O_3:Yb,Er (S3) nanoparticles and (B) magnetization curves of Fe_3O_4@SiO_2@Gd_2O_3:Yb,Er nanoparticles with different thickness of SiO_2 mid-layers obtained using obtained using (a) 0.53, (b) 2.67, (c) 5.34, (d) 13.35, and (e) 18.69 mL TEOS for preparation.

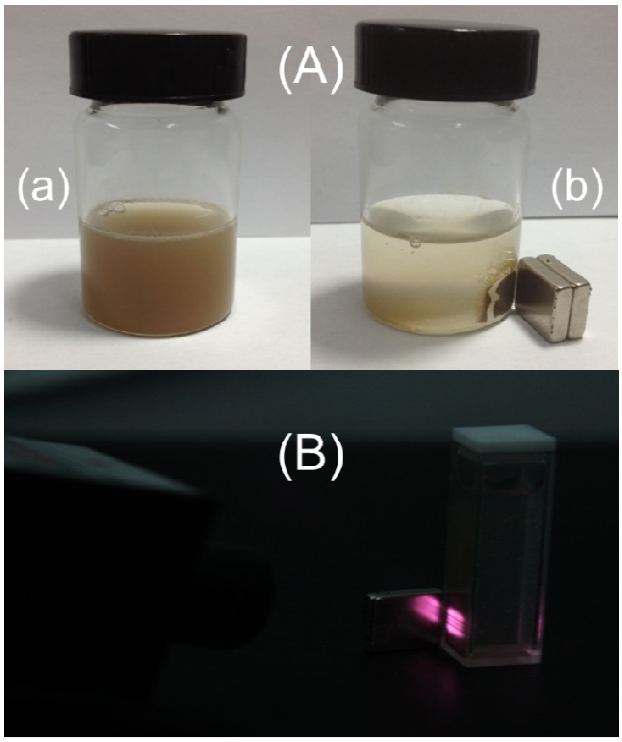

Figure 11. Photographs showing (A) aqueous solution of Fe_3O_4@SiO_2@Gd_2O_3:Yb,Er (S3) (a) before and (b) after magnetic separation and (B) red emission of the aqueous solution of Fe_3O_4@SiO_2@Gd_2O_3:Yb,Er (S3) under 980 nm excitation.

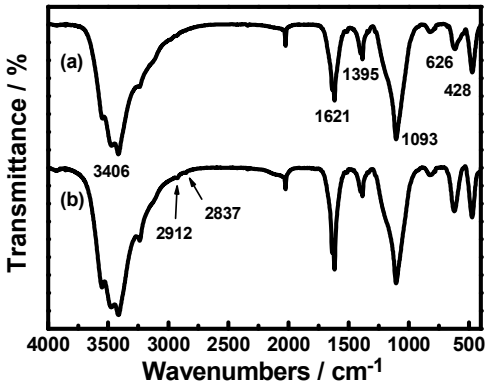

Figure 12. FTIR spectrums of (a) Fe_3O_4@SiO_2@Gd_2O_3:Yb,Er and (b) Fe_3O_4@SiO_2@Gd_2O_3:Yb,Er-NH_2.

Reference

1. V. Salgueiriño-Maceira, M. A. Correa-Duarte, M. Spasova, L. M. Liz-Marzán and M. Farle, *Advanced Functional Materials*, 2006, **16**, 509-514.
2. J. Kim, Y. Piao and T. Hyeon, *Chemical Society Reviews*, 2009, **38**, 372-390.
3. S. Gai, P. Yang, C. Li, W. Wang, Y. Dai, N. Niu and J. Lin, *Advanced Functional Materials*, 2010, **20**, 1166-1172.
4. H.-P. Zhou, C.-H. Xu, W. Sun and C.-H. Yan, *Advanced Functional Materials*, 2009, **19**, 3892-3900.
5. G. Wang, Q. Peng and Y. Li, *Accounts of Chemical Research*, 2011, **44**, 322-332.
6. N. M. Idris, Z. Li, L. Ye, E. K. Wei Sim, R. Mahendran, P. C.-L. Ho and Y. Zhang, *Biomaterials*, 2009, **30**, 5104-5113.
7. H. Hu, M. Yu, F. Li, Z. Chen, X. Gao, L. Xiong and C. Huang, *Chemistry of Materials*, 2008, **20**, 7003-7009.
8. Z. Liu, G. Yi, H. Zhang, J. Ding, Y. Zhang and J. Xue, *Chemical Communications*, 2008, 694.
9. J. H. Zeng, J. Su, Z. H. Li, R. X. Yan and Y. D. Li, *Advanced Materials*, 2005, **17**, 2119-2123.
10. L. Wang, R. Yan, Z. Huo, L. Wang, J. Zeng, J. Bao, X. Wang, Q. Peng and Y. Li, *Angewandte Chemie International Edition*, 2005, **44**, 6054-6057.
11. R. Abdul Jalil and Y. Zhang, *Biomaterials*, 2008, **29**, 4122-4128.
12. J. Shen, L.-D. Sun, Y.-W. Zhang and C.-H. Yan, *Chemical Communications*, 2010, **46**, 5731-5733.
13. L. Zhang, Y. S. Wang, Y. Yang, F. Zhang, W. F. Dong, S. Y. Zhou, W. H. Pei, H. D. Chen and H. B. Sun, *Chem Commun (Camb)*, 2012, **48**, 11238-11240.
14. X. Zhu, J. Zhou, M. Chen, M. Shi, W. Feng and F. Li, *Biomaterials*, 2012, **33**, 4618-4627.
15. X. Yu, Y. Shan, G. Li and K. Chen, *Journal of Materials Chemistry*, 2011, **21**, 8104-8109.
16. D. Hu, M. Chen, Y. Gao, F. Li and L. Wu, *Journal of Materials Chemistry*, 2011, **21**, 11276-11282.

17. Y. Zhang, S. Pan, X. Teng, Y. Luo and G. Li, *The Journal of Physical Chemistry C*, 2008, **112**, 9623-9626.
18. W. Li, Y. Deng, Z. Wu, X. Qian, J. Yang, Y. Wang, D. Gu, F. Zhang, B. Tu and D. Zhao, *Journal of the American Chemical Society*, 2011, **133**, 15830-15833.
19. T.-K. Tseng, J. Choi, M. Davidson and P. H. Holloway, *Journal of Materials Chemistry*, 2010, **20**, 6111-6115.
20. H. Sun, J. He, J. Wang, S.-Y. Zhang, C. Liu, T. Sritharan, S. Mhaisalkar, M.-Y. Han, D. Wang and H. Chen, *Journal of the American Chemical Society*, 2013, **135**, 9099-9110.
21. X. Niu, H. Li and G. Liu, *Journal of Molecular Catalysis A: Chemical*, 2005, **232**, 89-93.
22. N. C. Strandwitz and G. D. Stucky, *Chemistry of Materials*, 2009, **21**, 4577-4582.
23. L. Zhou, Z. Gu, X. Liu, W. Yin, G. Tian, L. Yan, S. Jin, W. Ren, G. Xing, W. Li, X. Chang, Z. Hu and Y. Zhao, *Journal of Materials Chemistry*, 2012, **22**, 966-974.
24. M.-H. Qu, R.-Z. Wang, Y. Chen, Y. Zhang, K.-Y. Li, H. Zhou and H. Yan, *Journal of Luminescence*, 2014, **148**, 181-185.
25. C. Zhao, X. Kong, X. Liu, L. Tu, F. Wu, Y. Zhang, K. Liu, Q. Zeng and H. Zhang, *Nanoscale*, 2013, **5**, 8084-8089.
26. C. Mi, J. Zhang, H. Gao, X. Wu, M. Wang, Y. Wu, Y. Di, Z. Xu, C. Mao and S. Xu, *Nanoscale*, 2010, **2**, 1141-1148.